WATER RESOURCES RESEARCH, VOL. 45, XXXXXX, doi:10.1029/2007WR006585, 2009

Sediment resuspension in a shallow lake

Eu Gene Chung,[1] Fabián A. Bombardelli,[1] and S. Geoffrey Schladow[1]

Received 10 October 2007; revised 31 January 2009; accepted 9 February 2009; published XX Month 2009.

[1] Different mathematical formulations for the computation of the entrainment rate of sediment into suspension in lakes can produce widely disparate results under a given set of conditions, leading to problematic interpretation. In this paper, the results of a 4-month field campaign on sediment resuspension in a large, shallow, hypereutrophic lake in southern California are presented. The field measurement program included the observation of currents and waves using a Nortek acoustic wave and current (AWAC) profiler, the observation of water temperatures using a thermistor chain, the use of optical backscatter sensors for the measurement of turbidity, a surrogate for suspended sediment concentration, and the use of meteorological data. The paper reports one of the first field experiments in lakes using the AWAC, whose signal strength has not been investigated in detail to date, and the correlation of a set of variables coming from different sources during a relatively long period of time. The contributions of different forcing mechanisms (waves, currents, and surface seiches) to the sediment resuspension in the lake are quantified, and the signal strength of the AWAC is used to address the vertical distribution of sediment in the water column. A novel relationship between the AWAC's backscatter intensity and turbidity is presented. Turbidity was found to be proportional to where w^K is the wind speed measured at 2 m and K ranged from 4.5 to 6.5, depending on the water depth. Finally, the results of modeling the sediment entrainment into suspension in the Salton Sea are shown to be well represented by an extension of the García and Parker formula.

Citation: Chung, E. G., F. A. Bombardelli, and S. G. Schladow (2009), Sediment resuspension in a shallow lake, *Water Resour. Res.*, *45*, XXXXXX, doi:10.1029/2007WR006585.

1. Introduction

[2] Many shallow lakes around the world have increasing loads of nutrients, heavy metals, and other toxic substances [*Linge and Oldham*, 2002; *Romero et al.*, 2002]. Sediment-water interactions in those lakes become increasingly important with time, since the bed sediments act as repositories for the added nutrients and toxic substances, which may eventually be released into the overlying water column. The upper layers of the bed sediments of shallow lakes participate in the exchange of substances with the water column through physical, chemical and biological processes and, very importantly, via sediment resuspension and horizontal sediment transport [*García*, 1999]. These upper layers can thus influence the cycling of nutrients, heavy metals and organic micropollutants in shallow lakes and reservoirs for a long time [*Blom et al.*, 1992].

[3] The prevalence of sediment resuspension in shallow, wind-exposed lakes has resulted in the development of many parametric models attempting to describe the relation between the hydrodynamics of water bodies and sediment resuspension rates [*Sheng and Lick*, 1979; *Aalderink et al.*, 1985; *Luettich et al.*, 1990; *Hamilton and Mitchell*, 1996; *Admiraal et al.*, 2000; *Sanford and Maa*, 2001; *Mian and Yanful*, 2004; *Cozar et al.*, 2005]. The rate of sediment resuspension (or entrainment rate of sediment into suspension) is quantified by ϕ_E, the vertical flux of solid particles close to the bottom. Dividing the entrainment rate by w_s, the terminal particle fall velocity in quiescent fluid, yields E_s, the nondimensional coefficient for entrainment of bed sediment into suspension [*García and Parker*, 1991, 1993; *Parker*, 2004; F. A. Bombardelli and M. H. García, Numerical simulation of wind-induced resuspension of bed sediment in sallow lakes, paper presented at the International Water Resources Engineering Conference, American Society of Civil Engineers, Seattle, Washington, 1999]. When the entrainment process is in equilibrium [*Admiraal et al.*, 2000; *Parker*, 2004], $E_s = c_{ae}$, where c_{ae} is the equilibrium near-bed sediment concentration (generally expressed in volume of sediment per unit volume of fluid, and measured at a certain distance a from the bottom).

[4] Most of the available models to compute E_s or ϕ_E agree upon establishing a dependence of the entrainment rate on the bottom shear stress induced by the motion of the attendant fluid, and also on the local sediment characteristics, usually through a given measure of the sediment size [*Sanford and Maa*, 2001]. *Aalderink et al.* [1985] put forward the following relation for sediment resuspension: $\phi_E \sim w^K$, where w indicates the wind speed at 10 m above the surface and K is an exponent which varies with the wind speed. *Mehta et al.* [1982], *Raudkivi* [1998] and *Sanford and Maa* [2001] reviewed a large number of formulae for the erosion rate of cohesive sediments, which can be

[1]Department of Civil and Environmental Engineering, University of California, Davis, California, USA.

0043-1397/09/2007WR006585$09.00

t1.1 **Table 1.** Some Recent Field Campaigns With Wave and Current Measurements

			Wave Measurements			Current Measurements		
t1.3	Authors	Location	Method	Frequency	Period	Method	Frequency	Period
t1.4	*Sheng and Lick* [1979]	Lake Erie, USA/Canada	water level gauges	-	3–5 Sep 1976	-	-	-
t1.5	*Luettich et al.* [1990]	Lake Balaton, Hungary	-	-	-	velocity meters, acoustic time-of-travel sensor	2 Hz	6–21 Aug 1985
t1.6	*Osborne and Greenwood* [1993]	Queensland Beach, St. Margaret's Bay, Nova Scotia, Canada	piezoelectric strain gauge transducers	4 Hz with 1 min break every 29 min	1324 h, 25 Oct 1987	biaxial electromagnetic current meter	4 Hz with 1 min break every 29 min	1324 h, 25 Oct 1987
t1.7		Bluewater Beach, Georgian Bay, Ontario, Canada	piezoelectric strain gauge transducers	5 Hz with 1 min break every 29 min	15 h, 3 Jun 1988	biaxial electromagnetic current meter	5 Hz with 1 min break every 29 min	15 h, 3 Jun 1988
t1.8	*Gloor et al.* [1994]	Lake Alpnach, Switzerland	-	-	-	acoustic current meter	every 1 min and every 5 min	8–22 May 1992
t1.9	*Hamilton and Mitchell* [1996]	Lake Ellesmere, New Zealand	pressure transducer	2 Hz (0.5 s interval), 6 records	Isolated events	-	-	-
t1.10	*Freire and Andrade* [1999]	Alfeite Beach in Tagus estuary, Portugal	two piezoresistive pressure transducers	-	17 Jun 1997, 10 records	-	-	-
t1.11	*Mian and Yanful* [2003]	Health Steele Mine Upper Cell, Canada	water level transducer	10, 20, 40 Hz, 1 h duration	for 3–6 times, 2–3 stations, July and August 1999	-	-	-
t1.12		Elliot Lake, Canada	water level transducer	10, 20, 40 Hz, 20 min duration	for 3–6 times, 4 stations, October 2000	-	-	-
t1.13	*Hawley et al.* [2004]	Lake Michigan, USA	pressure sensors	2 Hz or 4 Hz for 7 min every half hour	every half hour or hourly during the fall and winter in 1998-2000	-	-	-

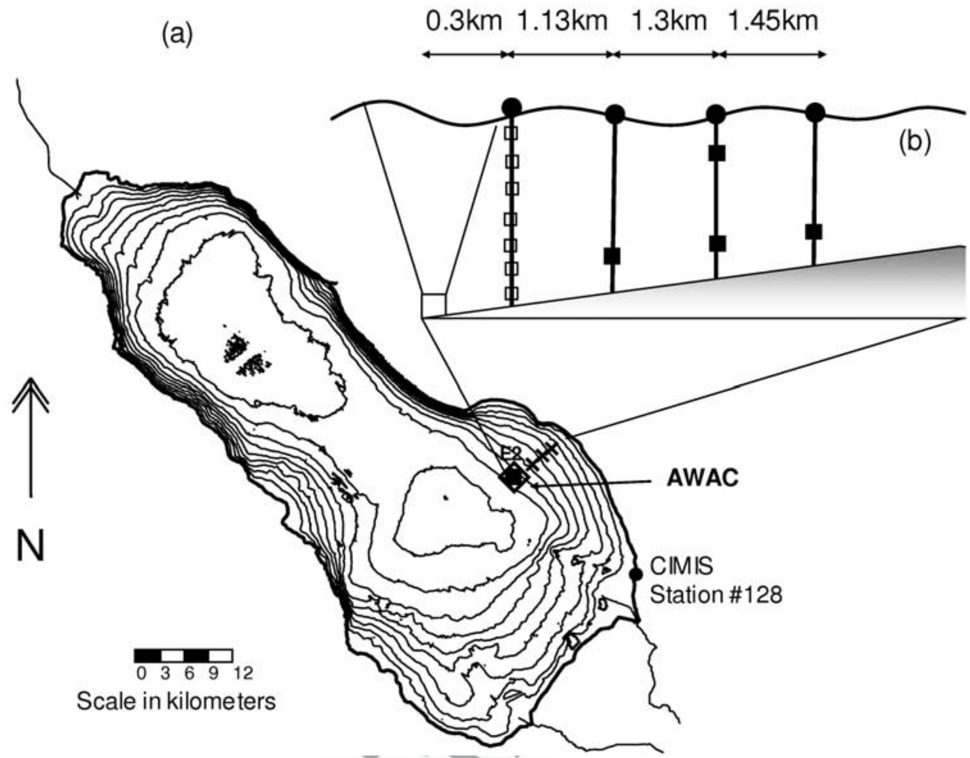

Figure 1. Location of sampling stations and bathymetry of the Salton Sea. (a) Bathymetry showing depth contours (at 1.52-m intervals). Shoreline elevation is −69.2 m relative to mean sea level (thick line). Square denotes the location of UC Davis thermistor chain; circle denotes locations of CIMIS meteorological station; crosses refer to the locations of the OBS stations; and diamond denotes the location of the AWAC profiler. (b) Schematic of the location of four YSI instruments, the AWAC, and the thermistor chain. The lake is located at approximately 33°N latitude and 115°W longitude.

subsumed under general expressions shown in Appendix A (see equation (A1)). There is also a vast body of formulations to compute the entrainment rate of sediment in open-channel flows [*García and Parker*, 1991; *García*, 1999]. Most of the relations for E_s are of the following type:

$$E_S \sim \phi_E \sim \tau_b^P \sim u_*^{2P} \sim w^K \qquad (1)$$

where τ_b and u_* are the bed shear stress and the wall friction (shear) velocity due to skin friction, respectively, and P and K are empirical exponents. These relations for open-channel flows have been obtained under steady state, equilibrium conditions (or, moderate disequilibrium conditions), for essentially unimodal, noncohesive sediment particles, and for a uniform distribution of the shear stress in space. One such relation is the expression by *García and Parker* [1991, 1993] for noncohesive sediment, also presented in Appendix A (see equation (A2)).

[5] On the basis of a thorough review of the literature on the subject of sediment resuspension, the relations coming from open-channel flows have not been tested in lakes. In spite of the inherent differences between the boundary layers in open-channel and lake flows, this is somewhat surprising, especially considering the fact that these expressions have been derived mainly using dimensional analysis. Moreover, it turns out that the formulations for the computation of the sediment entrainment rate can produce widely disparate results under the same set of conditions, which adds to the inherent complexity of understanding sediment-related processes in lakes.

Table 2. Period and Frequency of Data Sampling

			Data Frequency[a]	
Instrument/Data Source	Measurement Data	Period	Reading	Recording
YSI/OBS	turbidity	4 Aug to 26 Sep 2005	15 min	15 min
AWAC	wave height, direction and period, current magnitude and direction, pressure	4 Aug to 29 Nov 2005	7 Hz	30 min
			4.34 Hz	10 min
Thermistor chain	water temperature	2 Aug to 25 Nov 2005	10 min	10 min
CIMIS	air temperature, wind speed, wind direction	continuous	1 min	60 min

[a]The frequency of data recording was different from the frequency of data reading in order to save battery resources and memory.

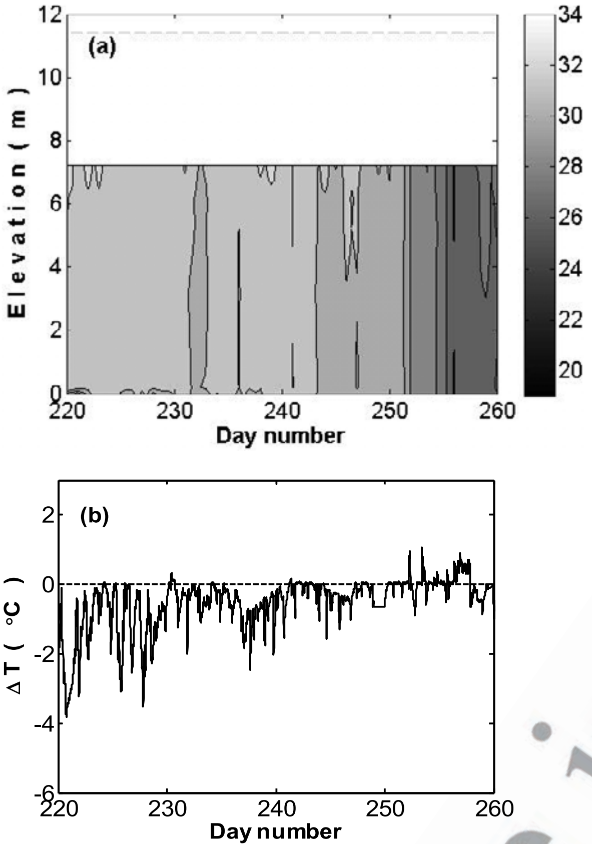

Figure 2. (a) Observed temperatures (°C) at station E2. The dashed line shows water surface. The upper portion of the data is missing because of instrument malfunction. (b) Temperature differences ($\Delta T = T_{lower} - T_{upper}$, in °C) between bottom and top thermistors at station E2. Negative ΔT values imply lower temperature with increasing depth, which is thermodynamically stable. Positive ΔT indicates an inverse temperature gradient.

[6] On the other hand, to observe sediment resuspension, sediment concentrations are usually measured close to the bottom, under the hypothesis that quasi-equilibrium conditions are prevalent. This measurement is undertaken either continuously, by using beam transmissometers or optical backscatter (OBS) sensors [*Gloor et al.*, 1994; *James et al.*, 1997; *Jin and Wang*, 1998; *Weyhenmeyer et al.*, 1995], or in an integrated way by using sediment traps [*Evans*, 1994; *Jurg*, 1996; *Kozerski*, 1994; *Lindstrom et al.*, 1999; *Rosa et al.*, 1983].

[7] In this paper, the results of a 4-month field experiment on sediment resuspension in a large, shallow, hypereutrophic lake, the Salton Sea in southern California, are presented. The field measurement program included the observation of currents and waves using a Nortek acoustic wave and current (AWAC) profiler, the observation of water temperatures using a thermistor chain, the use of OBS sensors for the measurement of turbidity, a surrogate for suspended sediment concentration [*Gippel*, 1989; *Suk et al.*, 1998; *Cozar et al.*, 2005], and the use of meteorological data. The paper reports one of the first field campaigns in lakes using the AWAC, whose signal strength has not been investigated in detail to date, and the correlation of a set of variables coming from different sources during a relatively long period of time (section 2.1; cf. Table 1). In section 3.1, the contribution of different forcing mechanisms (waves, currents and surface seiches) to the sediment resuspension in the lake is quantified, and the signal strength of the AWAC is used to address the vertical distribution of sediment in the water column. Section 3.1 also puts forward novel relations between the AWAC's backscatter intensity and turbidity. Finally, section 3.2 presents the modeling of sediment entrainment into suspension in the Salton Sea by introducing an extension of the García and Parker formula.

2. Experiment Design and Methods

2.1. Instrument Deployment

[8] The Salton Sea is a highly saline (44‰ salinity), eutrophic and shallow lake located east of San Diego, California, USA. Its length is over 56 km along a northwest/southeast axis, and its width is 24 km. It has an area of 963 km^2, with a maximum depth of 15.5 m (Figure 1). The lake is characterized by high nutrient concentrations, high algal biomass as demonstrated by high chlorophyll *a* concentrations, high fish productivity, low clarity, frequent very low dissolved oxygen concentrations, massive fish kills, and noxious odors [*Holdren and Montaño*, 2002].

[9] The instruments were deployed in the southeastern portion of the Salton Sea (Figure 1a) on the basis of the prevailing west-southwest wind direction and previous modeling that suggested high potential for resuspension in this region [*Anderson*, 2003]. Turbidity data came from three observation stations containing Yellow Springs Instruments (YSI) Inc. six-series multiparameter probes equipped with OBS sensors [*Gippel*, 1989; *Suk et al.*, 1998; *Cozar et al.*, 2005]. Wave and current data came from the in situ Nortek AWAC. Water temperature came from HOBO temperature loggers attached to a thermistor chain. Meteorological data were taken from a California irrigation management information system (CIMIS) station located at the southeast of the Sea (Figure 1a).

[10] Four OBS sensors were deployed at three sites with water depths of 4, 6, and 8 m, respectively, as shown in Figure 1b, from 4 August 2005 to 26 September 2005. They were placed 0.5 m off the bottom at each station. The 6 m station had an additional OBS 5 m off the bottom. The sampling interval was 15 min. Each sensor had a wiper blade to minimize the effect of biofouling and barnacle growth.

[11] The Nortek AWAC provided near-continuous profiles of current magnitude and direction (at 0.75 m vertical increments), and wave height, direction and period. The AWAC was located 100 m away from a thermistor chain at station E2 as shown in Figure 1. The AWAC sampled at frequencies of 7 Hz for wave characteristics and 4.34 Hz for currents from 4 August 2005 to 29 November 2005. The data sampled at these frequencies were averaged and recorded at 30- and 10-min intervals for waves and currents, respectively, to extend battery duration and memory. The instrument mounting frame and the "blanking distance" precluded velocity measurements in the first 1.8 m above the bottom [*Nortek*, 2004]. STORM, software provided by Nortek, was used for acquiring and processing AWAC data.

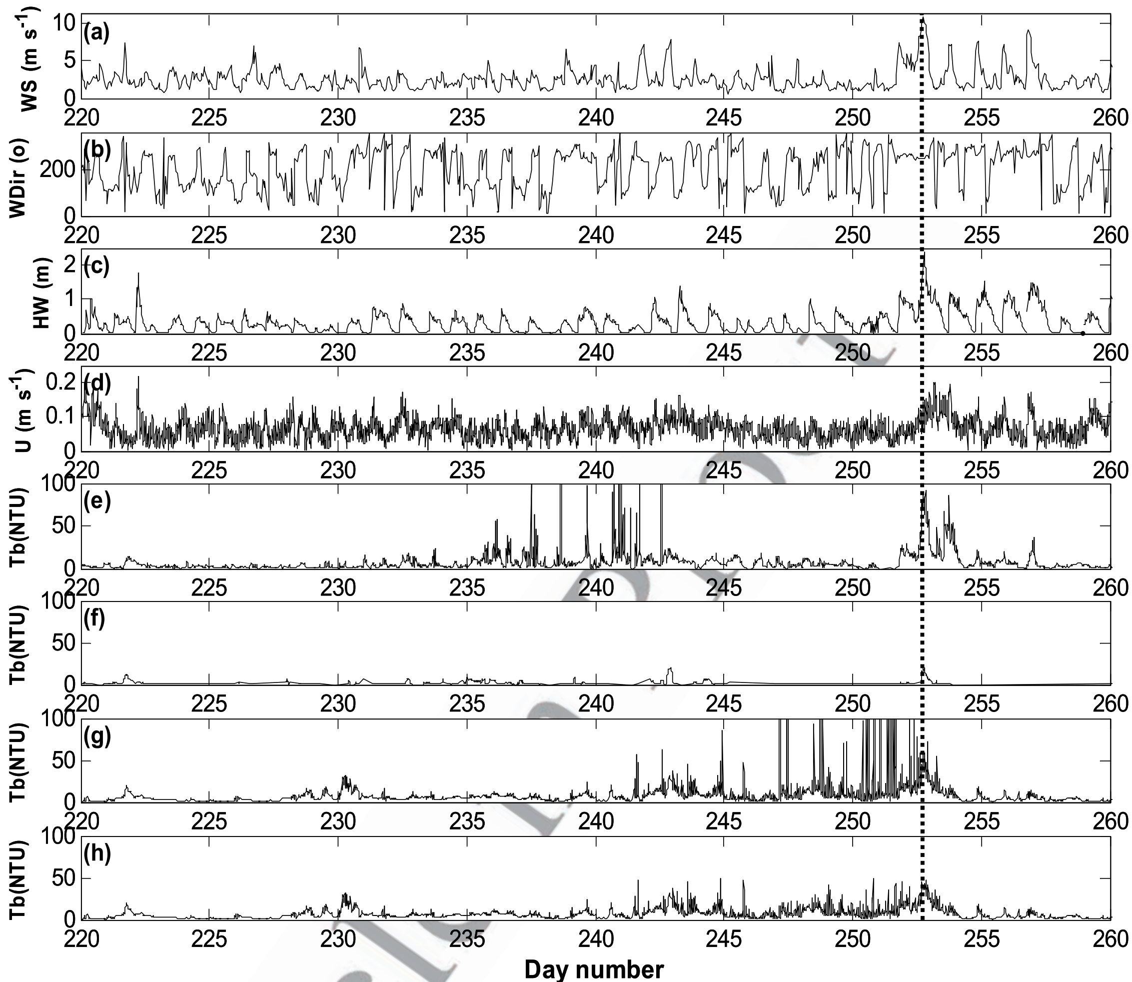

Figure 3. Comparison of variables from 8 August to 17 September 2005: (a) wind speed (WS, m s^{-1}), (b) wind direction (Wdir, degrees from the north), (c) significant wave height (HW, m), (d) current speed (U, m s^{-1}) at 1.8 m from the bottom, (e) turbidity (Tb) 0.5 m off the bottom in depth of 4 m (NTU), (f) turbidity (Tb) 5.5 m off the bottom in depth of 6 m (NTU), (g) turbidity (Tb) 0.5 m off the bottom in depth of 6 m (NTU), and (h) turbidity (Tb) <50 NTU 0.5 m off the bottom in depth of 6 m (NTU). Each data set is presented at the frequency at which it was stored. The vertical line highlights the simultaneous occurrence of peaks in several variables.

[12] The thermistor chain at station E2, recorded from 2 August 2005 to 25 November 2005. The thermistor chain had 7 temperature loggers located at 0, 0.2, 3.2, 5.2, 6.2, 7.2, and 8.2 m above the lake bed; a surface temperature logger malfunctioned during the observation period. The sampling interval was 10 min.

[13] Wind data were taken from CIMIS station 128. Solar radiation, air temperature, relative humidity, and wind velocity and direction are recorded at 1 h intervals. Wind data is measured at 2 m above ground level, and wind direction is denoted in degrees clockwise from the north. Table 2 summarizes the data used.

[14] The sediment characteristics of the Salton Sea were analyzed by *Anderson* [2003], who provided the average sediment size distribution for the entire lake, and *Vogl and Henry* [2002], who provided demarcations of percentages of sand, silt, and clay in the Sea. For the area of interest, the bed sediment is 35% sand, 40% silt, and 25% clay. This corresponds to a minimum grain size of 23 μm and a maximum grain size of 400 μm [*Parker*, 2004]. It is noteworthy that 10% composition by clay particles might be sufficient to render the sediment behavior as cohesive [*Raudkivi*, 1998].

2.2. Expressions for the Computation of the Bed Shear Stress due to Currents and Waves

[15] Bed shear stresses due to wind-induced currents in open-channel flows can be computed with the vertical distribution of horizontal velocities (see F. A. Bombardelli and A. N. Menéndez, A physics-based, quasi-3-D model for wind-induced shallow water flows, paper presented at the International Water Resources Engineering Conference, American Society of Civil Engineers, Seattle, Washington, 1999). For lakes, computing reliable values for the bed shear stress is more complicated, given the spatial and temporal variation of the shear stresses. Waves and currents may induce shear stresses in different directions, in which case the shear stresses have to be added in vector form [*Horikawa*, 1978; *Nielsen*, 1992; *Raudkivi*, 1998]. The magnitude of the bottom shear stress due to currents, τ_{curr},

Table 3. Relations Between Turbidity and Total Suspended Solids

Authors	Location	Equation	Units: TSS Range	Units: TURB	Note
		Lakes			
Chow-Fraser [1999]	Lake Ontario	log10(TSS) = 0.665(±0.035) × log10 (TURB) + 0.716	mg L^{-1} (up to 400)	FTU	40 FTU = 29 NTU [*Gippel*, 1989]
Knowlton and Jones [1995]	Mark Twain Lake	TSS = 0.932 × TURB + 0.0038*TURB^2	mg L^{-1} (up to 1000)	NTU	
Wang et al. [2003]	Lake Okeechobee	TSS = 1.2807 × TURB − 36.933	mg L^{-1} (up to 250)	mg/L	
		Streams and Creeks			
Chanson et al. [2006]	Eprapah Creek (Australia)	TSS = 4.85 × TURB − 35	mg L^{-1} (up to 800)	NTU	lab test
Gippel [1995]	Eden catchment, Victoria (Australia)	TURB = 0.84 × TSS + 4.62	mg L^{-1} (up to 153)	NTU	

may be approximated as a fraction (about 10%, [*Reid*, 1957]) of the surface, wind-induced shear stress [*Mian and Yanful*, 2004]. The wind-induced shear stress at the surface of the lake, τ_0, is in turn usually estimated using a quadratic drag law. Thus,

$$|\tau_{curr}| = 0.1\tau_0 = 0.1 C_D \rho_a w_{10}^2 \quad (2)$$

where ρ_a denotes the density of air and the drag coefficient $C_D = 0.001\ (0.75 + 0.0\ 67\ w_{10})$, where w_{10} is the velocity of the wind at 10 m above the water surface. Given the range of flows close to the bottom, this is obviously a simplification of a very complicated problem, but given the small fraction of the shear stress due to currents

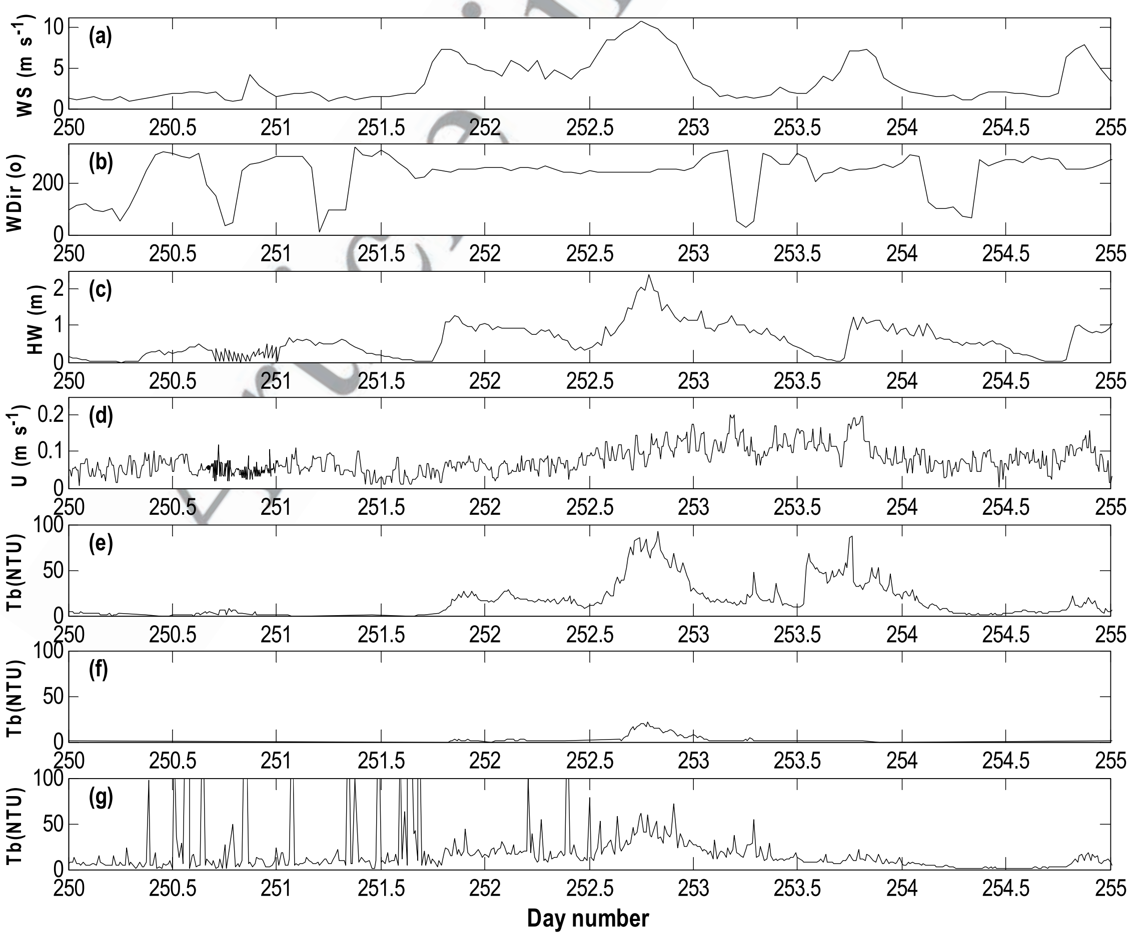

Figure 4. Comparison among variables from 7 to 12 September 2005: (a) wind speed (WS, m s^{-1}), (b) wind direction (Wdir, degrees from the north), (c) significant wave height (HW, m), (d) current speed (U, m s^{-1}) at 1.8 m from the bottom, (e) turbidity (Tb) 0.5 m off the bottom at a depth of 4 m (NTU), (f) turbidity (Tb) 5.5 m off the bottom at a depth of 6 m (NTU), and (g) turbidity (Tb) 0.5 m off the bottom at a depth of 6 m (NTU). Each data set is presented at the frequency at which it was stored.

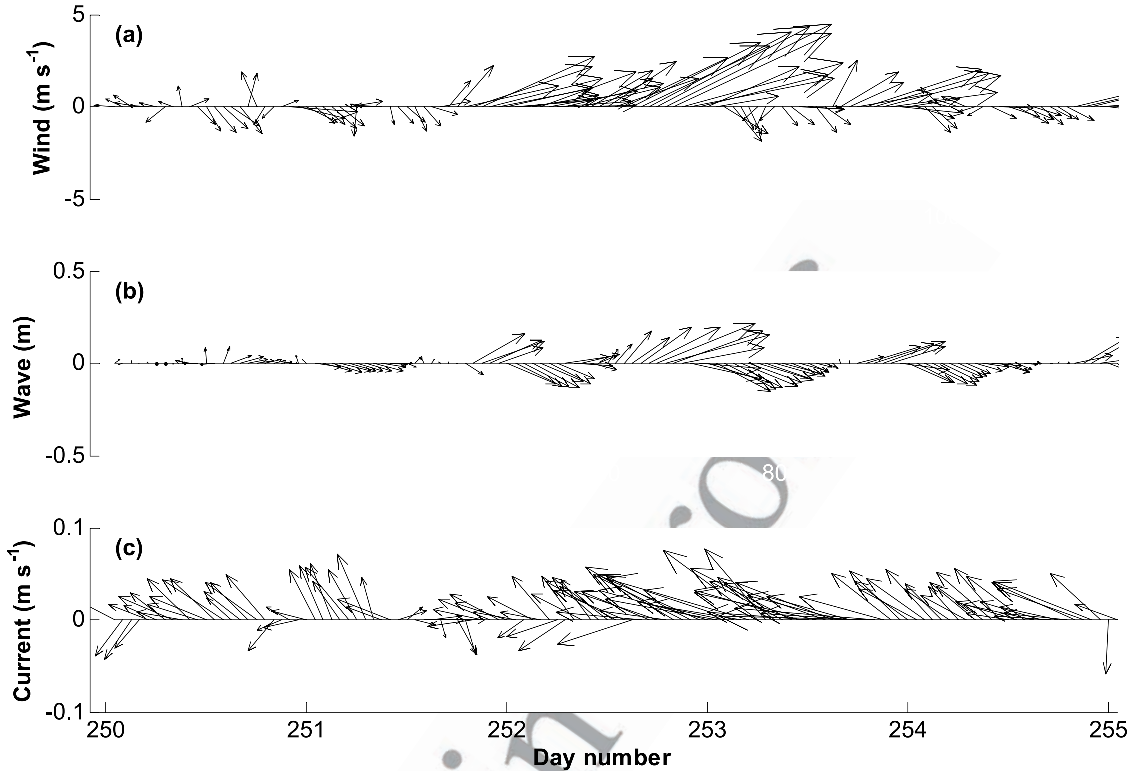

Figure 5. Vector plot of variables from 7 to 12 September 2005: (a) wind speed, (b) waves, and (c) currents at 1.8 above bottom.

compared to waves (see below), it was considered to be satisfactory.

[16] The maximum shear stress exerted on the bottom sediments due to wind-induced waves, τ_{wave}, can be calculated as [*Raudkivi*, 1998; *Mian and Yanful*, 2004]

$$|\tau_{wave}| = 0.5\rho f_W U_W^2 \tag{3}$$

where ρ is the water density; U_w is the amplitude of the wave orbital velocity, given by the small-amplitude wave theory as $U_W = \frac{H_w \pi}{T_w \sinh\left(\frac{2\pi H}{L_W}\right)}$; f_w is the bottom friction factor, $f_W = \frac{2}{\sqrt{R_W}}$ (valid for the viscous-dominated regime, which extends up to wave Reynolds numbers of about 10^4, [*Kamphuis*, 1975; *Luettich et al.*, 1990; *Sanford*, 1992; *Smyth and Hay*, 2002]); R_w denotes the Reynolds number, $R_W = \frac{U_W A_W}{\nu}$; A_w is the maximum displacement of the individual fluid particles from their mean position, $A_W = \frac{U_W}{\omega}$; $\omega = \frac{2\pi}{T_w}$ is the wave angular frequency; ν is the kinematic viscosity of water; and H_w, T_w, and L_w denote the height, period, and length of the wave, respectively. In turn, H indicates water depth.

2.3. Expressions for the Critical Shear Stress

[17] The critical shear stress of equation (A1) has been given various meanings by different authors. P. D. Komar and M. C. Miller (Sediment threshold under oscillatory waves, paper presented at the 14th Coastal Engineering Conference, American Society of Civil Engineers, Copenhagen, 1974) and *Madsen and Grant* [1975] showed that diverse empirical data for incipient motion in oscillatory flows agree well with *Shields* [1936] diagram if the shear stress is calculated with the bed friction factor, f_w, as above [*Raudkivi*, 1998, p. 343]. However, in lacustrine environments, benthic communities could stabilize or bioturbate the bed depending on the level of activity of these communities, and the critical shear stress could be very different than that given by Shields-type curves. In cases where there is not enough information to assess this, the critical bottom shear stresses can be estimated from $\tau_{cr} = \tau_c^* \ \rho \ R \ g \ D$, where $R = \frac{\rho_s - \rho}{\rho}$ (the submerged specific gravity), ρ_s is the sediment density, D denotes the sediment grain size, and g is the acceleration of gravity. The critical (nondimensional) Shields' parameter, τ_c^*, can be obtained employing well-known curve fittings to *Shields* [1936] experimental data set for incipient sediment motion developed by *Parker et al.* [2003] and *Parker* [2004]:

$$\tau_c^* = 0.5\left[0.22\mathrm{Re}_p^{-0.6} + 0.06 \quad 10^{\left(-7.7\mathrm{Re}_p^{-0.6}\right)}\right] \tag{4}$$

where $\mathrm{Re}_p = \sqrt{gRDD}/\nu$, with ν denoting the kinematic viscosity of water.

3. Results and Discussion

3.1. Data Analysis and Interpretation

3.1.1. Time Series Data Analysis

[18] Temperature profiles were used to assess the degree of thermal stratification in the lake. *Cook* [2000] observed that the salinity in the Salton Sea is usually homogenous in

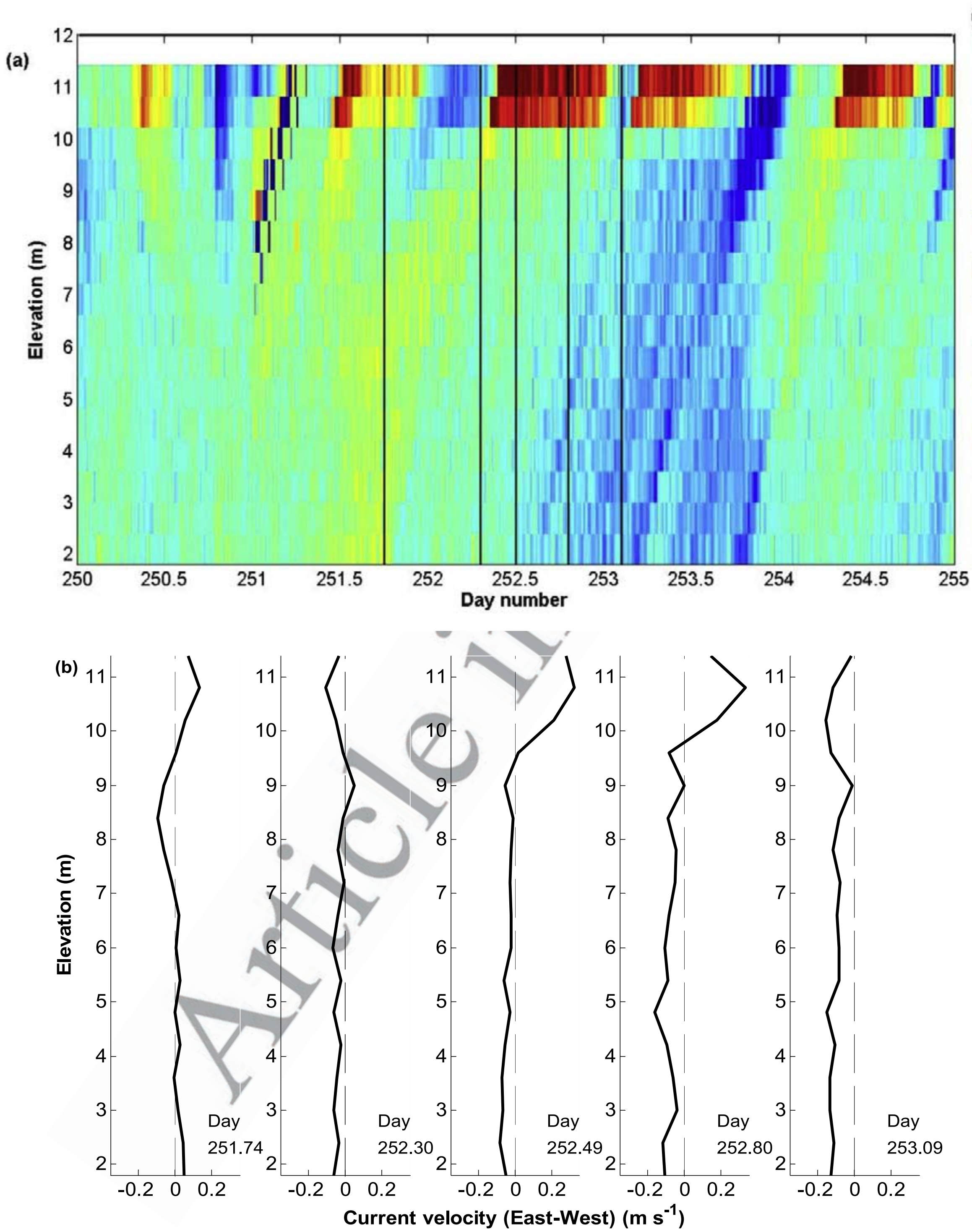

Figure 6. Flow velocity observed with the AWAC for the east-west direction: (a) elevation-time contours of flow velocity (m s^{-1}) during days 250–255 and (b) vertical profiles of flow velocity for different specific times indicated with solid vertical lines in Figure 6a.

the vertical direction and, therefore, haline stratification is not of concern Auxiliary material.[1] Temperatures through most of the water column were in excess of 25°C from August until early September (Figure 2a). Mixing of the whole water column occurred during part of most days between day numbers 232–260 (20 August 2005 to 17 September 2005) at station E2 (Figure 2b), consistent with observations of *Holdren and Montaño* [2002].

[19] Figure 3 shows a compilation of the measurements undertaken at the Salton Sea. Raw values of turbidity (expressed in NTU) larger than 1,000 were intermittently

[1]Auxiliary materials are available in the HTML. doi:10.1029/2007WR006585.

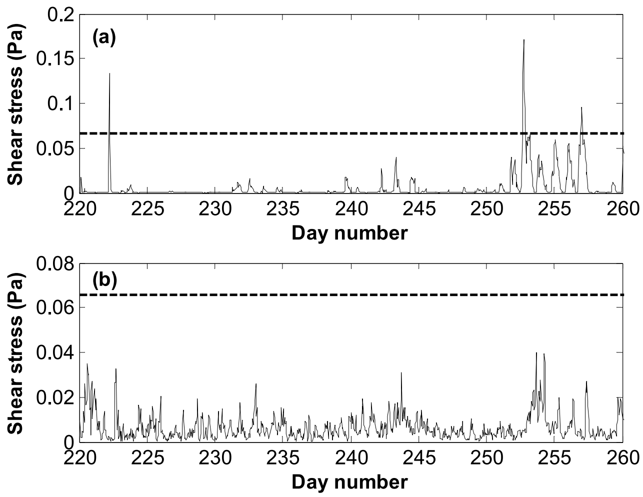

Figure 7. Comparison of bed shear stress generated by (a) waves and (b) currents, computed from data collected by the AWAC. The dashed line at 6.25×10^{-2} Pa corresponds to the critical bed shear stress for incipient motion corresponding to an average particle size of 25 μm.

recorded during the measurement period, especially at the 8-m station. These values appeared during periods without strong winds and waves, and were considered to be unrealistically high. These were eventually attributed to a sporadic malfunction of the wiper blade attached to the OBS sensors, whereby it occasionally stopped on the optical window, partially obscuring it and leading to spurious backscatter values. As a partial check on this explanation, formulae that relate turbidity values to concentrations of suspended sediment are presented in Table 3. Using the formulae for lakes given by *Knowlton and Jones* [1995], for example, a value of sediment concentration of 1,000 mg L^{-1} corresponded to 405 NTU. This value is much higher than values observed by *Holdren and Montaño* [2002] in the Salton Sea (ranging from 9 to less than 200 mg L^{-1}). Therefore, recorded values of turbidity larger than 500 NTU were disregarded in our analysis (Figures 3e, 3f, and 3g). In Figure 3h, a cutoff of 50 NTU is used, and there appears to be virtually no change to the underlying turbidity signal exhibited during high wind periods. Singular spikes still remain (for example, for days 237–243 at the 4-m station), which could still be attributable to malfunction of the wiper blade.

[20] Most of the observation period was calm or had moderate winds, with the exception of days 251–258 (8–15 September 2005). At about day 252.5, maxima of both wind speed and significant wave height were observed (about 12 m s^{-1} and 2.1 m, respectively). Further, clear peaks in turbidity at the 4-m and 6-m stations were also observed. However, maximum values of current speed of 0.2 m s^{-1} were observed a day later at day 253.5.

[21] Details of the same data for the period between days 250–255 are shown in Figures 4 and 5. Wind shows a quasi-constant direction (from the west) between days 251.8 and 253. Figure 5 also shows that while wave direction tends to follow rather closely the wind direction, the current direction at 1.8 m from the bottom is at 90 to 180° to the wind direction.

[22] Time series analysis of these data reveals that the occurrence of peaks in wave height can be clearly associated with peaks in wind speed, denoting an evident cause-effect relation. However, the timing of peaks in the current record does not agree with those for peaks in the wind record. This delay of almost 1 day could be attributed to the time it takes to produce the large-scale cyclonic (counterclockwise) gyre that characterizes the southern portion of the Salton Sea [*Cook et al.*, 2002]. The peaks of wind speed, wave height and turbidity appear to coincide, confirming that waves are the predominant mechanism for sediment resuspension. There are some peaks in turbidity which do not correspond to relatively high winds or high waves, such as those from days 235 to 245 for the 4-m station (Figure 3e) or days 240–250 for the 6-m station (Figure 3g). This might be the result of small resuspension events generated close to the shore or the wiper blade malfunction alluded to previously.

[23] Figure 6a presents the elevation-time distribution of the east-west current velocity component from the AWAC for days 250–255. Velocities are on the order of 0.03 m s^{-1} most of the time, with values in the range 0.15–0.2 m s^{-1} during days 252–254. Similar values of velocity at the sampling locations were observed by *Cook et al.* [2002] in numerical simulations. Figure 6b in turn shows a set of vertical profiles of current velocity, in the east-west direction, from days 251–253. When the wind increases from days 252 to 252.75, a boundary layer develops close to the free surface, and deepens, as expected, with the concomitant recirculation close to the bottom. As time progresses, this boundary layer disappears with declining winds, also as expected.

3.1.2. Computation of Bed Shear Stresses From Measurements

[24] The water density in equation (3), ρ, has to account for the high temperatures, high salinity, and

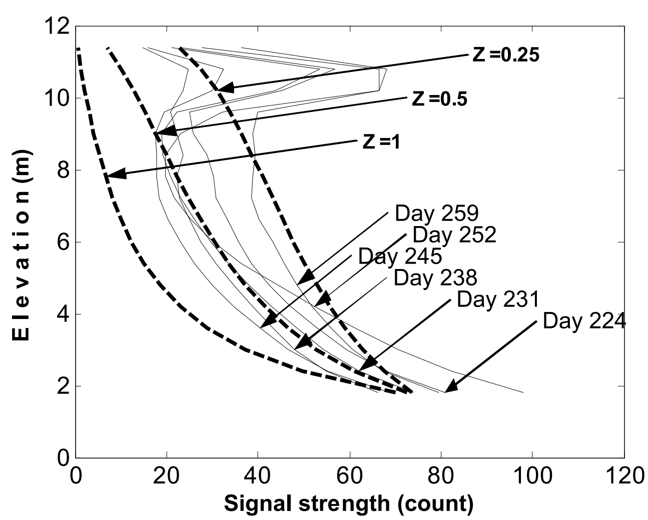

Figure 8. Comparison among daily averaged signal strength (count) profiles and the Rousean distribution. Thin black lines are signal strength profiles observed every 7 days from days 224 to 259, and the dashed lines represent the Rousean distribution. Large values of the signal strength on the upper part of the depth can be attributed to sidelobe interference.

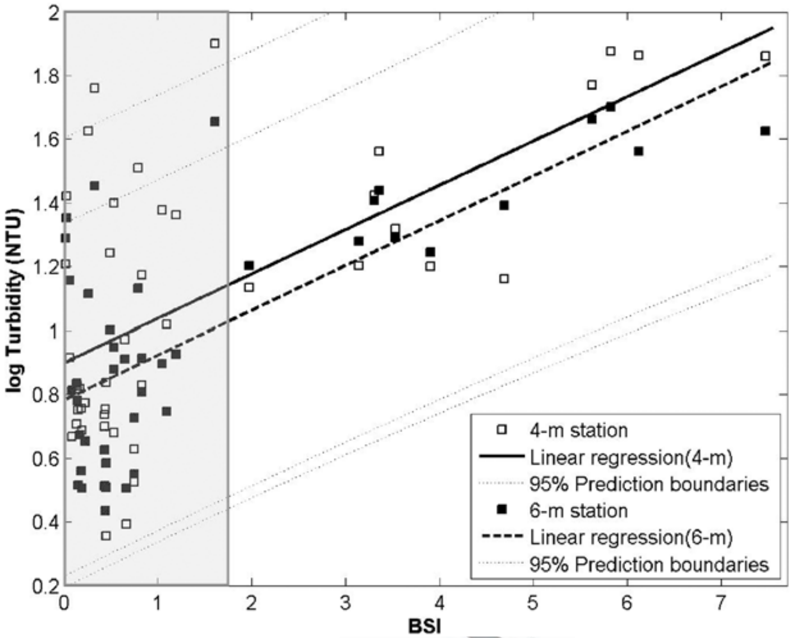

Figure 9. Linear regressions of the base 10 logarithm of turbidity (NTU) versus backscatter intensity (*BSI*) of the AWAC, including data from the 4-m station and 0.5 m off the 6-m station. The shaded region indicates data corresponding to *BSI* < 1.8 with a significant scatter. Open squares denote turbidity from the 4-m station; solid squares denote turbidity from the 6-m bottom station.

suspended sediment in the Salton Sea. Adopting well-known expressions compiled by *Gill* [1982] and *Wüest et al.* [1992], we computed the density in the Salton Sea for an average value of salinity of 40 parts per thousand [*Tostrud*, 1997] and an average concentration of suspended sediment of 40 mg L^{-1} [*Holdren and Montaño*, 2002], obtaining a density of 1026 kg m^{-3} at 28°C [see also *Bombardelli and García*, 2001]. The kinematic viscosity of water, ν, was assumed to be 0.82×10^{-6} m^2 s^{-1}. (Typical environment variations of viscosity with salinity are much smaller than those with temperature.) For the density of air, a value of 1.16 kg m^{-3} was assumed.

[25] Figure 7 compares the bed shear stresses due to waves and currents, calculated from measured values of wind speed, wave height and wavelength using equations (2) and (3). Wind speeds were adjusted from 2 m to 10 m using the semilogarithmic velocity law [*Cook*, 2000]. As expected, the shear stresses induced by waves are higher than those driven by currents, as consistently found in other shallow lakes [*Luettich et al.*, 1990; *Hawley*, 2004; *Mian and Yanful*, 2004]. The dashed line indicates the critical bottom shear stress of 6.25×10^{-2} Pa, obtained for a sediment size of 25 μm, a value considered representative for the Salton Sea (see below). The wave shear stresses exceeded the critical shear stress during the period from day 250–255. Those computations include the evaluation of the wave Reynolds number. For all times, R_w was below 10^4 [*Kamphuis*, 1975], confirming the hypothesis of a viscous-dominated flow regime. In Appendix B, we show that other forcing, such as surface seiches, do not contribute to the sediment resuspension.

3.1.3. Interpretation of Signal Strength From AWAC

[26] Acoustic sensors such as the AWAC detect acoustic reflections from particles in suspension; therefore, the signal strength can provide information about the quantity and type of particulate matter in the water column [*Lohrmann*, 2001]. Sediment concentrations in open-channel flows under equilibrium conditions are characterized by the Rousean distribution:

$$c = c_{ae}\left[\frac{(H-z)/z}{(H-a)/a}\right]^Z \tag{5}$$

Table 4. Exponents for Relations of Sediment Entrainment as a Function of Bed Shear Stress for Equation (1)

Author	*P*	K
Noncohesive Sediment		
García and Parker [1991]	2.5	5
Akiyama and Fukushima [1986]	5	10
Van Rijn [1984]	1.5	3
Celik and Rodi [1984]	1.5	3
Zyserman and Fredsoe [1994]	1.75	3.5
Cohesive Sediment		
Mian and Yanful [2004]	2	4
Sanford and Maa [2001]	1	2
Maa et al. [1998]	1.5–3.6	3–7.2
Kandiah [1974] and *Arulanandan* [1975]	1	2
Mehta (1981)[a]	1	2
Thorn and Parsons (1980)[b]	1	2

[a]A. J. Mehta, Review of erosion function for cohesive sediment beds, paper presented at First Indian Conference on Ocean Engineering, Indian Institute of Technology, Madras, India, 1981.

[b]M. F. C. Thorn and J. C. Parsons, Erosion of cohesive sediments in estuaries: An engineering guide, paper presented at 3rd International Symposium on Dredging Technology, BHRA Fluid Engineering, Bordeaux, France, 1980.

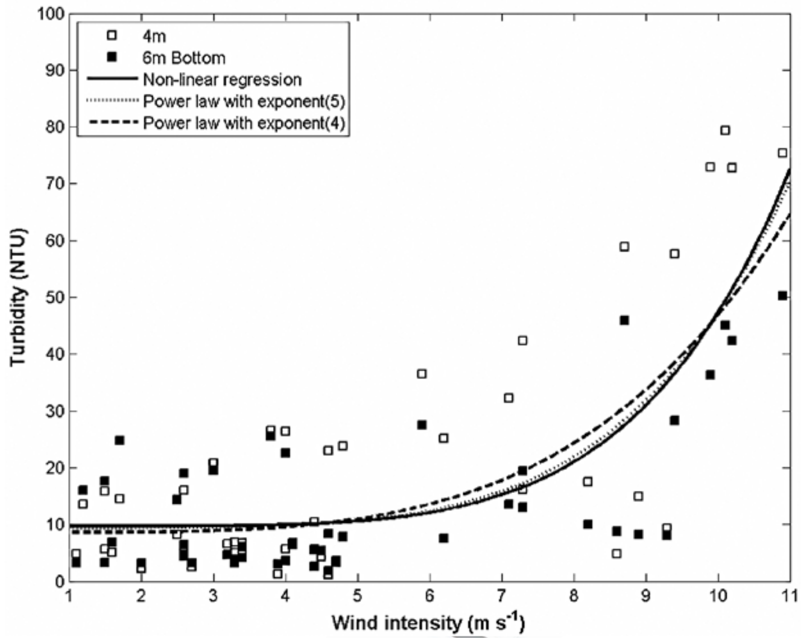

Figure 10. Nonlinear regressions of turbidity versus wind speed, including data from the 4-m station (empty squares) and 6-m bottom station (solid squares) (R^2 = 0.57). Also included are relations obtained by fixing exponents equal to 4 (R^2 = 0.56) and 5 (R^2 = 0.57).

where the dimensionless Rouse number is defined as

$$Z = \frac{w_s}{\kappa u_*} \tag{6}$$

c is the local volume concentration of suspended sediment (averaged over turbulence), z is the vertical distance above the bed, and κ is the von Kármán constant [*Julien*, 1998; *García*, 1999]. The Rousean distribution indicates a balance between the upward flux of sediment due to turbulence and the effect of gravity returning particles to the bed. The Rousean profile has been also found to be a plausible model for the wave-averaged sediment distribution in the vertical in coastal areas (see *Raudkivi* [1998, p. 361], *Hsu et al.* [2003], and Appendix C).

[27] The profiles of the daily averaged signal strength (in counts) obtained from the AWAC every 3 days from day 224 to day 257 are compared in Figure 8 with the Rousean distribution [*Hsu et al.*, 2003; *Raudkivi*, 1998]. It is assumed that counts at different elevations are proportional to sediment concentration [*Chanson et al.*, 2006]. An arbitrary concentration was assumed at a depth of 2 m to generate the Rousean distributions. The profiles of daily averaged values of signal strength do not differ significantly from the instantaneous profiles of signal strength. For a value of Z = 0.5, the shape of the Rousean profile closely resembles that of the signal strength, particularly in the lower 6 m. This suggests that the conditions for suspended sediment in the Salton Sea during the observation period were close to equilibrium or to mild disequilibrium, and that the resuspension of sediment is mostly a local phenomenon with isolated episodes of horizontal transport. The value of the sediment particle diameter that produces Z = 0.5 in equation (6) varies between 9 and 42 μm, depending on the local shear velocity [*Parker*, 2004]. This range of sediment sizes coincides with the range of sediment sizes discussed in section 2.1, and justifies the value of 25 μm employed previously.

[28] Despite the fact that the AWAC was some kilometers away from the OBS sensors (see Figure 1a), the relationship between the signal strength of AWAC and turbidity was examined. The signal strength amplitude can be related to the dimensionless acoustic backscatter intensity (*BSI*) as $BSI = P_1\ 10^{0.0434.AMP}$, where *AMP* denotes the backscatter amplitude (in counts) and P_1 is a sensor/sediment coefficient chosen to be 1×10^{-5} to provide a bound for *BSI* [*Chanson et al.*, 2006; *Nikora and Goring*, 2002]. Following *Gartner* [2004] and *Chanson et al.* [2006], we can postulate

$$\log_{10}(SSC) \sim \log_{10}(TURB) = A + B\,BSI \tag{7}$$

where A and B are empirically derived coefficients and *SSC* denotes the suspended solids concentration. Figure 9 shows the relation between the logarithm of turbidity at the 4-m and 6-m (bottom) stations and the *BSI* estimated from the signal strength at 1.8 m from the bottom. The points displayed in Figure 9 pertain to conditions in which the shear stress was larger than the critical shear stress. Data corresponding to $BSI < 1.8$ show a large amount of scatter. For $BSI \geq 1.8$, a linear trend can be clearly identified (R^2 values for the 4-m and 6-m stations are 0.37 and 0.51, respectively). The slope of the regression, B, is the same for bottom turbidity at both the 4-m and 6-m stations, and is equal to 0.14 (approximately 1/7).

3.1.4. Development of Relations Between Hydrodynamic Variables and Turbidity From Observations in the Salton Sea

[29] Equation (1), developed for open-channel flows, presented the functional relationship between entrainment

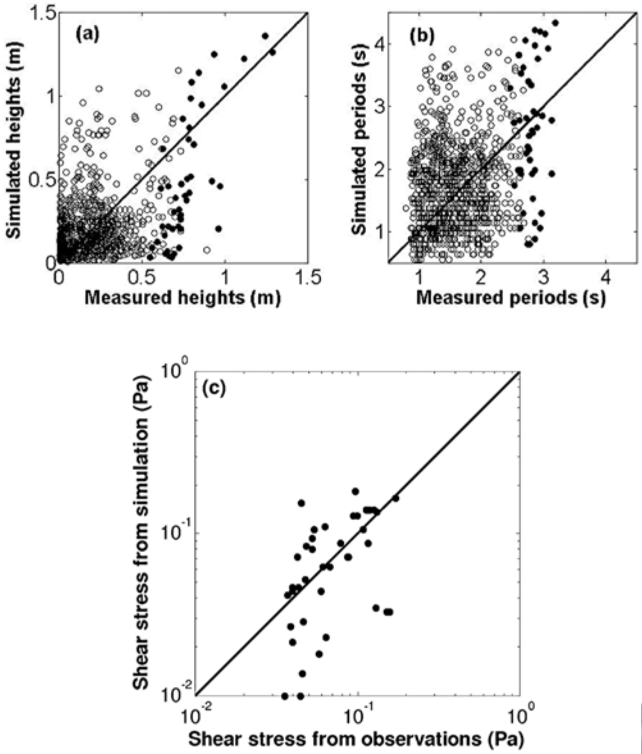

Figure 11. Comparison between measured and simulated wave characteristics in the observation area: (a) significant wave height (m) and (b) wave period (s). We denoted with different symbols those points corresponding to conditions in which the bed shear stress computed with the measured wave heights was smaller (open circles) or larger (solid circles) than the critical shear stress. (c) Comparison of shear stresses induced by waves for times when the bed shear stress exceeded the critical shear stress. Measured bottom shear stresses were obtained with observed wave heights and periods.

and either bed shear stress or wind speed. A range of values for the exponents for bed shear stress and wind speed (*P* and *K*, respectively) are presented in Table 4 for both cohesive and noncohesive sediments, using the scaling presented in Appendix A. The exponent *K* ranges from 2 to 10 for both currents and waves. The range of *K* values is larger for noncohesive sediments (3 to 10) than for cohesive sediments (2 to 7.2).

[30] Given the variability of exponents in Table 4, the performances of two particular exponent values against data of the Salton Sea were compared. Figure 10 shows turbidity at 4-m and 6-m bottom stations versus hourly wind speeds (m s^{-1}) from CIMIS station 128. Data were from those times at which the bed shear stress was larger than the critical shear stress. The plot shows regressions to the data points using exponent values of 4 and 5. A regression to the data of the type: $TURB\ (NTU) = d\ [w(m\ s^{-1})]^K + c$, where *d*, *K* and *c* are coefficients, was also determined. The estimated exponents (coefficients *K*) at each station were 4.76 at the 4-m station, 6.40 at the 6-m bottom station, and 5.39 considering both stations, which are within the range of reviewed exponents in Table 4.

[31] *Maa et al.* [1998] observed exponents *P* ranging from 1.5 to 3.6 (corresponding to *K* values from 3.0 to 7.2) for large shear stress values for cohesive sediment. *Lick et al.* [2007] obtained *P* values ranging from 1.37 to 3.59 (*K* varying from 2.74 to 7.18) for quartz particles with different percentages of clay minerals. *Keen and Furukawa* [2007] obtained good results for cohesive sediments in a range of water bodies, employing $P = 3$ ($K = 6$). Notice that the exponents obtained for the Salton Sea are within the range obtained by all the authors above. It is also possible to observe in Figure 10 that the regression for a fixed exponent equal to 5 (which follows the *García and Parker* [1993] relation, equation (A2) produces a good representation of the data points, considering the natural scatter of sediment-related phenomena, and the fact that the exponent pertains to a formula that was devised for noncohesive sediment. Notably, the regression with an exponent equal to 4 (following the equation by *Mian and Yanful* [2004], equation (A1), with $m = 2$) also provides a good approximation of the data points. On the basis of this result, these formulas are employed in our parametric model.

3.2. Simulation of Sediment Resuspension

3.2.1. Modeling of Bed Shear Stresses

[32] The Sverdrup-Munk-Bretschneider (SMB) model for shallow water waves [*Sheng and Lick*, 1979; *Coastal Engineering Research Center* (*CERC*), 1984] was applied to calculate the wave parameters in the Sea. The model estimates wave heights and periods for given values of wind speed and fetch. Wavelengths were computed iteratively on the basis of the wave theory, as a function of the depth and the computed period.

[33] Using an effective fetch of 30 km at the observation stations following *CERC* [1984], the simulated wave heights and periods were compared with the observed values in Figure 11. The model was able to predict significant wave heights reasonably well, while the predictions of significant wave periods had a relatively large scatter, as noticed by other researchers (see [*Hawley et al.*, 2004]). This large scatter may have a detrimental effect on the

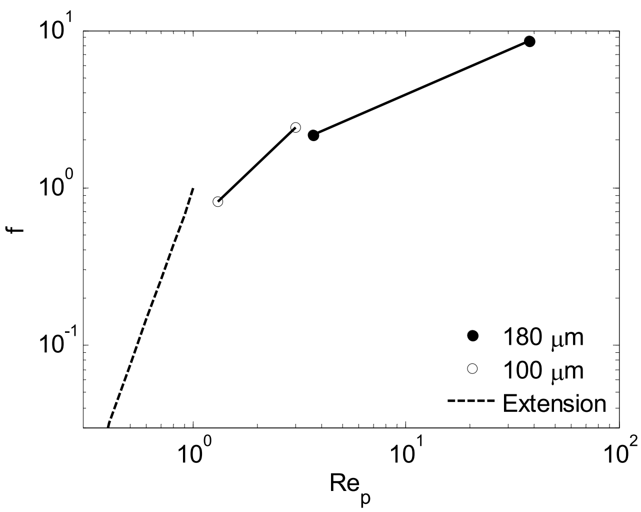

Figure 12. Extension (dashed line) of measurements of *García and Parker* [1993] for $0.4 < Rep < 1$. Circles indicate the measured points by García and Parker.

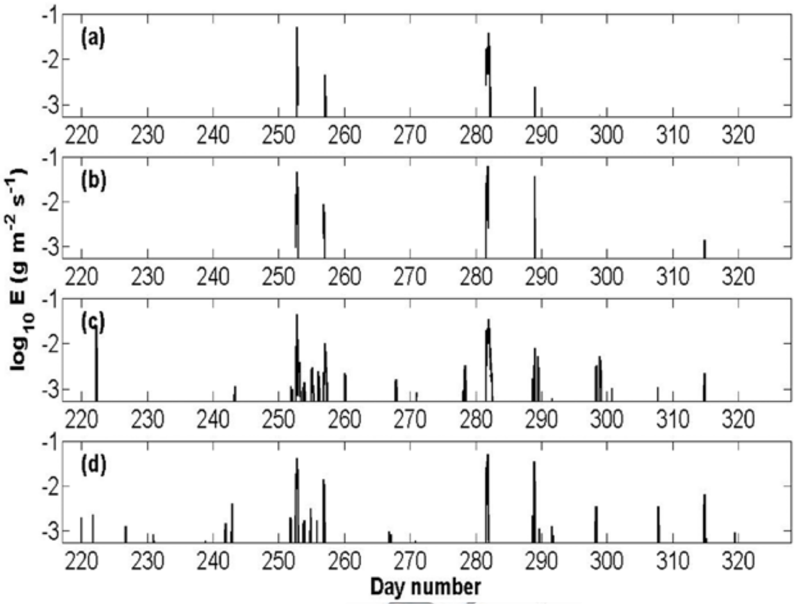

Figure 13. Comparison among sediment entrainment rates simulated using the *Mian and Yanful* [2004] and the extended García and Parker formulas: (a) sediment entrainment rate using the expression of *Mian and Yanful* [2004] employing simulated wave parameters, (b) sediment entrainment rate using the *Mian and Yanful* [2004] formula employing measured wave parameters, (c) sediment entrainment rate using the extended García and Parker formula employing simulated wave parameters, and (d) sediment entrainment rate using the extended García and Parker formula employing measured wave parameters.

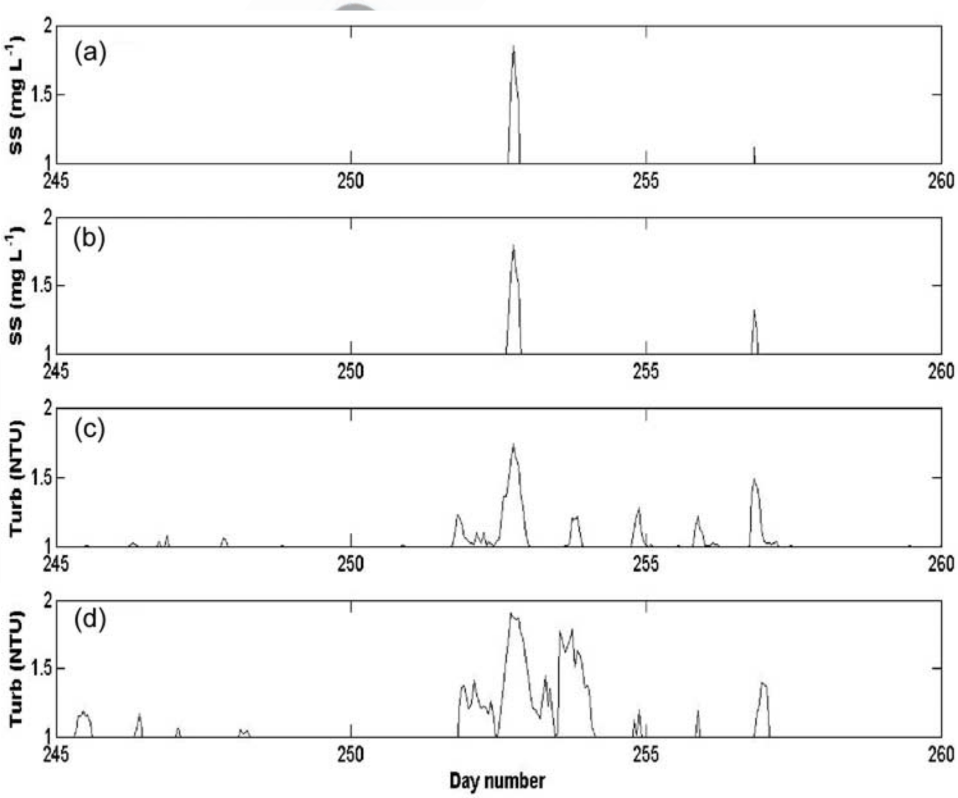

Figure 14. Comparison among simulated and inferred sediment entrained into suspension at the bottom of the 4-m station: (a) the base 10 logarithm of suspended sediment concentration (SS) simulated using the expression of *Mian and Yanful* [2004], (b) the base 10 logarithm of suspended sediment concentration (SS) simulated using the expression of the extended García and Parker formula, (c) the base 10 logarithm of simulated turbidity (Turb) using the nonlinear regression (NTU) of section 3.1.4, and (d) the base 10 logarithm of measured turbidity (Turb) at the 4-m station (NTU).

computation of the bed shear stresses according to equations given in section 2.2; however, it was found that the influence of the scatter of the wave period was not so severe in this case, as demonstrated in Figure 11c where we compare modeled versus "measured" bed shear stresses generated by waves only, with relatively good agreement for the larger stresses (>5 $\times$ 10^{-2} Pa) as opposed to the lower ones ("Measured" bed shear stresses were computed with observed wave heights.).

3.2.2. Modeling of Sediment Entrainment Into Suspension. Extension of the García and Parker Formula

[34] Using the sediment size of 25 μm, the value of Re_p is smaller than 1, which is beyond the limits of application of the *García and Parker* [1993] formula (1 < Re_p < 3). In this work, we extended the formula of García and Parker to the conditions of the Salton Sea, using values of Rep smaller than 1 but larger than 0.4 (Figure 12). We proposed the following relation: $f(\mathrm{Re}_p) = \mathrm{Re}_p^{3.75}$ (for 0.4 < Re_p < 1) which provides a smooth extension of the data points of *García and Parker* [1993].

[35] Figure 13 compares entrainment rates predicted by using the *Mian and Yanful* [2004] and the extended García and Parker formulations, obtained with simulated (Figures 13a and 13c) and measured (Figures 13b and 13d) wave characteristics for the whole observation period. Figure 13 indicates satisfactory agreement between predictions with both formulas, particularly at higher entrainment levels. The results obtained using the extended García and Parker formulation included some events of small entrainment rates, which did not appear in the results obtained with the *Mian and Yanful* [2004] formula (see Figures 13c and 13d).

[36] Figure 14 compares the simulated sediment concentrations by using the two equations (Figures 14a and 14b), the simulated turbidities by using the nonlinear regression between turbidity and wind speed of section 3.1.4 (Figure 14c), and the measured turbidity at the 4-m station (Figure 14d). It can be seen that the two models compute the peak at day 252.5 of about 60–70 mg L^{-1}, which agrees satisfactorily with the peak of about 50 NTU obtained from the application of the nonlinear regression. (The equivalence between mg L^{-1} and NTU was provided by the formula of *Knowlton and Jones* [1995]; see Table 3.) Obviously, since this model uses a cause-effect relation, it cannot predict some of the peaks in sediment concentration outside of days 250–255.

4. Conclusions

[37] The observations presented in this paper constitute the most complete data set on sediment resuspension in the Salton Sea. They have been obtained via the synchronization of the AWAC, OBS sensors, and a thermistor chain. The present set of observations differs from previous measurements in that a comprehensive set of variables have been simultaneously and continuously monitored in the Salton Sea for a relatively long period. The AWAC also proved to be a reliable and useful instrument to be used in harsh environmental conditions such as those found in the Salton Sea. Although more research is obviously needed, this study shows that the AWAC signal strength can be used to assess the existence of quasi-equilibrium conditions for the suspension of sediments in a lake, and to assess the potential of surface seiches.

[38] The boundary layers in open-channel and in lake flows differ significantly, given their intrinsic physical features and their diverse space and time scales. Consequently, resuspension events are essentially different in both types of flow. However, when wave-induced flows in lakes are analyzed from an averaged perspective of thousands of wave periods, as done in this work, the resuspension phenomena in lakes and open channels begin to look surprisingly similar. This suggests that resuspension formulas devised for open-channel flows can be adapted/extended for use in wave-induced flows in lakes.

[39] Nonlinear relations between wind speed and turbidity developed in this study suggested exponents for the wind speed between 4.5 to 6.5 (depending on water depth) which are consistent with relations found in the literature. In addition, a relation between turbidity and a surrogate of the backscatter intensity (*BSI*) of the AWAC was developed. And this logarithmic relation shows a reasonable robustness despite the natural scatter of the data.

[40] An extension of the formula for sediment resuspension by García and Parker was suggested for the Salton Sea. Ongoing research is devoted to analyze the validity of this formula to compute the rate of sediment entrained into suspension in other shallow lakes.

Appendix A: Sediment Resuspension Formulae

[41] Most expressions to quantify sediment resuspension for cohesive sediments are of the type [*Mehta et al.*, 1982; *Raudkivi*, 1998; *Sanford and Maa*, 2001]

$$\begin{array}{ll} E = \alpha\left[\frac{\tau_b - \tau_{cr}}{\tau_{cr}}\right]^m & \mathit{for}\,\tau_b \geq \tau_{cr} \\ E = 0 & \mathit{for}\,\tau_b < \tau_{cr} \end{array} \tag{A1}$$

where E is the net, specific rate of entrainment of sediment in units of mass area^{-1} time^{-1}; α is a coefficient; m is an exponent ranging from 1 to 3.6 [*Raudkivi*, 1998; *Maa et al.*, 1998]; and τ_{cr} is the critical shear stress. The exponent is given as 2 in the equation by *Mian and Yanful* [2004].

[42] *García and Parker* [1993] formula is given by

$$E_s = \frac{AZ_u^5}{\left(1 + \frac{A}{0.3}Z_u^5\right)} \tag{A2}$$

where A is a constant equal to 1.3 $\times$ 10^{-7}; $Z_u = \frac{u_*}{w_s} f\left(\mathrm{Re}_p\right)$, where $\mathrm{Re}_p = \frac{\sqrt{gRD^3}}{\nu}$ (the explicit particle Reynolds number), $R = \frac{\rho_s - \rho}{\rho}$ (the submerged specific gravity), ρ is the water density, and ρ_s is the sediment density; D denotes the sediment grain size; g is the acceleration of gravity; ν is the kinematic viscosity of water; and $f(\mathrm{Re}_p) = 0.586\ \mathrm{Re}_p^{123}$. This formula is valid for 1 < Re_p < 3, and applies at a distance of 1/20th of the water depth. The relation by *García and Parker* [1991] was later tested for flow pulses by *Admiraal et al.* [2000], who corroborated that the formula can give satisfactory predictions in unsteady conditions as long as a time delay is applied to account for the lag between the bed shear stress and the entrainment.

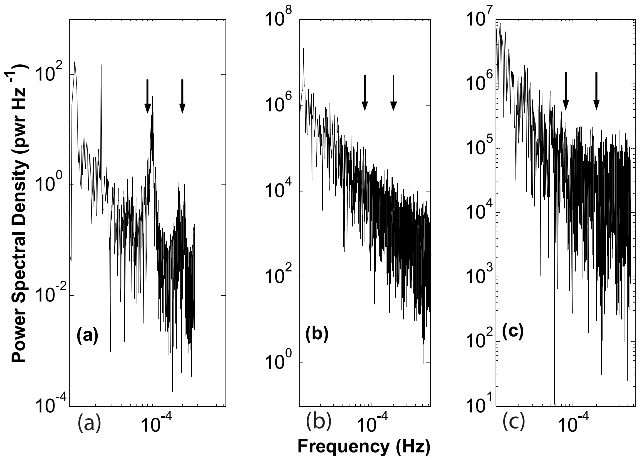

Figure B1. Power spectral density (power Hz^{-1}) from 7 August to 17 September 2005: (a) pressure (m), (b) signal strength (counts) from the lowest AWAC bin, and (c) turbidity (NTU) at station of depth 4 m. The arrows indicate the theoretical frequency values of the first-mode surface seiches (8×10^{-5} and 2×10^{-4} Hz) corresponding to the length and width of the Salton Sea.

[43] Rearranging (A2) yields

$$E_s = \frac{A}{\left(\frac{1}{Z_u^5} + \frac{A}{0.3}\right)} \tag{A3}$$

As Z_u is O(10), $\frac{1}{Z_u^5}$ is O(10^{-5}) whereas $\frac{A}{0.3}$ is O(10^{-7}). We can therefore conclude that $E_s \sim Z_u^5$. On the other hand, $u_* \sim \tau_b^{1/2}$ by definition; thus, $Z_u \sim \tau_b^{1/2}$ or $E_s \sim \tau_b^{5/2}$. The bed shear stress for currents scales as the square of the wind speed; therefore, $E_s \sim w^5$. From these relations we conclude that $P = 2.5$ and $K = 5$.

Appendix B: Potential Occurrence of Surface Seiches in the Salton Sea

[44] Wavelengths (λ_{Seiche}) and angular frequencies (ω_{Seiche}) of surface seiches in the Sea were estimated using the dispersion relation [*Kundu and Cohen*, 2004]

$$\lambda_{Seiche} = \frac{2L}{n+1}; n = 0, 1, 2, \ldots \tag{B1}$$

$$\omega_{Seiche} = \sqrt{\frac{\pi g(n+1)}{L} \tanh\left(\frac{(n+1)\pi H}{L}\right)}; n = 0, 1, 2, \ldots \tag{B2}$$

where L is the length scale of the water body, and n refers to the normal mode of the seiche. Using the length and width of the Salton Sea (56 and 24 km, respectively) as length scales, equation (B2) yields frequencies ($f_{Seiche} = \omega_{Seiche}/2\pi$) of 8×10^{-5} and 2×10^{-4} Hz for the first mode seiche. Power spectra of the AWAC hydrostatic pressure, the AWAC signal strength from the lowest bin (1.8 m), and the turbidity sensor at the 4-m station for the period 7 August 2005 to 17 September 2005 were produced (Figure B1). Peaks in the pressure signal power spectral density (PSD) are evident close to the two first mode frequencies suggesting that the Salton Sea had significant surface seiches during the sampling period. However, there are no corresponding peaks in the PSD of signal strength or turbidity, indicating no influence of surface seiches on sediment resuspension and turbidity.

Appendix C: Conditions for the Rousean Distribution to be Valid in a Lake

[45] Several authors have presented information on the vertical profiles of sediment concentration in coastal areas around the world. These profiles, which are time averaged in the wave period, have consistently shown a decrease of the concentration with the distance from the bed. *Raudkivi* [1998, p. 361] summarizes different formulations to describe such concentration distributions, including (1) a simple exponential decay with the distance from the bed, (2) power expressions, and (3) the Rousean distribution. *Horikawa* [1978] included a derivation of the concentration distribution (p. 266) and an extended discussion of different formulations for the vertical sediment distribution (p. 268). His results yielded a similar form to what we refer to as a Rousean distribution. Thus, the equilibrium Rousean distribution appears to be a widely accepted profile, valid in coastal areas.

[46] A criterion to assess the conditions under which the Rousean distribution is valid in a lake can be obtained from the advection-diffusion equation for sediment in suspension averaged over turbulence [*Parker*, 2004], as follows:

$$\frac{\partial c}{\partial t} + \frac{\partial}{\partial x_j}\left(\overline{v_j} c\right) - w_s \frac{\partial c}{\partial z} = -\frac{\partial}{\partial x_j}\left(\overline{v_j' c'}\right) \tag{C1}$$

where c indicates the local sediment concentration, which is a function of time and space; ν refers to the water velocity; the overbar indicates an average over turbulence; w_s is the particle fall velocity; z is the vertical distance above the bed; and summation is implied on the subscript j. In (C1), the molecular diffusion terms have been disregarded. Equation (C1) can be integrated over a wave period, giving

$$\int_{t_0}^{t_0+T} \frac{\partial c}{\partial t} dt + \int_{t_0}^{t_0+T} \frac{\partial}{\partial x_j}\left(\overline{v_j} c\right) dt - \int_{t_0}^{t_0+T} w_s \frac{\partial c}{\partial z} dt = -\int_{t_0}^{t_0+T} \frac{\partial}{\partial x_j}\left(\overline{v_j' c'}\right) dt \tag{C2}$$

Applying Leibnitz's rule, and disregarding the spatial variations of the wave period in the observation area, it is possible to obtain the following expression, where the angle brackets indicate wave-averaged variables, and T_w refers to the wave period

$$c\Big|_{t_0}^{t_0+T} + \frac{\partial}{\partial x_j}\left(\left\langle \overline{v_j} c \right\rangle T_w\right) - w_s \frac{\partial(\langle c \rangle T_w)}{\partial z} = -\frac{\partial}{\partial x_j}\left(\left\langle \overline{v_j' c'} \right\rangle T_w\right) \tag{C3}$$

The local concentration of sediment can be expected to be similar at the beginning and the end of the wave period for regular waves. Also, the vertical component of the water velocity can be neglected relative to the horizontal ones. Under those conditions, the vertical balance between the settling of particles and the effect of turbulence embedded in the Rousean concept is attained when the terms associated with the horizontal transport are much smaller than the vertical ones, as follows:

$$\frac{\frac{\partial}{\partial x}\left(\langle \overline{v_j} c\rangle T_w\right)}{w_s \frac{\partial(\langle c\rangle T_w)}{\partial z}} \sim \frac{\frac{1}{L} U_e c_e}{w_s \frac{1}{H} c_e} = \frac{H}{L}\frac{U_e}{w_s} << 1 \qquad \text{(C4)}$$

where the subscript e refers to scale variables, and L and H indicate a horizontal length scale and the water depth. Adopting the following values for the Salton Sea: $H = 5$ m, $U_e = 0.01$ m s^{-1}, and $w_s = 0.0005$ m s^{-1}, $L = 10{,}000$ m, the above ratio is much smaller than unity. Thus, the application of the Rousean distribution for the Salton Sea is basically sound.

Notation

ϕ_E vertical turbulent Reynolds flux of solid particles close to the bottom, m s^{-1}.
λ_{Seiche} wavelength of seiche, m.
ρ water density, kg m^{-3}.
ρ_a air density, kg m^{-3}.
ρ_s sediment density, kg m^{-3}.
τ^* Shields parameter, dimensionless.
τ_c^* critical Shields parameter, dimensionless.
τ_b bed shear stress, Pa.
τ_{cr} critical shear stress, Pa.
τ_{wave} maximum shear stress exerted on the bottom sediments due to wind-induced waves, Pa.
ν kinematic viscosity of water, m^2 s^{-1}.
ω_{Seiche} angular frequency of seiches in the lake, rad s^{-1}.
A constant in the *García and Parker* [1991, 1993] formula, dimensionless.
A_W maximum displacement of the individual fluid particles from their mean position, m.
d, coefficients in the nonlinear regression for turbidity versus wind speed.
a distance of the measurement point of sediment concentration with respect to the lake bottom, m.
c_{ae} mean equilibrium near-bed concentration of sediment, volume of sediment/total volume.
c local, mean volume concentration of suspended sediment, volume of sediment/total volume.
C_D drag coefficient in the expression for the shear stress from wind, dimensionless.
D sediment grain size, μm.
E net specific entrainment rate of sediment into suspension, g area^{-1} time^{-1}.
E_s dimensionless coefficient of entrainment of bed sediment into suspension.
g acceleration of gravity, m s^{-2}.
f_{Seiche} frequency of seiche, Hz.
f_W bottom friction factor, dimensionless.
H water depth, m.
H_w wave height, m.
K exponent of wind speed in its relation with E_s.
L length scale of the lake, m.
L_W wavelength, m.
m exponent in erosion rate for cohesive sediments.
P e exponent of bed shear stress in its relation with E_s.
Re_p explicit particle Reynolds number, dimensionless.
R submerged specific gravity, dimensionless.
R_W wave Reynolds number, defined as $R_W = \frac{U_W A_W}{\nu}$, dimensionless.
ΔT inverse temperature gradient, °C.
T_w wave period, s.
u_* shear (wall friction) velocity due to skin friction, m s^{-1}.
w_{10} wind speed at 10 m above the water surface, m s^{-1}.
U_W amplitude of the wave orbital velocity, m s^{-1}.
w wind speed, m s^{-1}.
w_s terminal (fall) particle velocity in quiescent fluid, m s^{-1}.
Z Rouse number, dimensionless.
z vertical distance above the bed, m.

[47] **Acknowledgments.** This research was supported by the University of California Water Resources Center and by the California Department of Water Resources (DWR). We are also grateful to comments provided by David H. Schoellhamer from UC Davis and the U.S. Geological Survey (USGS) on early versions of the manuscript. We thank Bill Sluis and Daret Kehlet of UC Davis for their help with the instrument deployment in the Salton Sea and Jack Crayon of the California Department of Fish and Game for providing logistical support and local knowledge.

References

Aalderink, R. H., L. Lijklema, J. Breukelman, W. Vanraaphorst, and A. G. Brinkman (1985), Quantification of wind induced resuspension in a shallow lake, *Water Sci. Technol.*, *17*, 903–914.
Admiraal, D. M., M. H. García, and J. F. Rodriguez (2000), Entrainment response of bed sediment to time-varying flows, *Water Resour. Res.*, *36*, 335–348, doi:10.1029/1999WR900227.
Akiyama, J., and Y. Fukushima (1986), Entrainment of noncohesive sediment into suspension, in *Proceedings of the 3rd International Symposium on River Sedimentation*, edited by S. Y. Wang, H. W. Shen, and L. Z. Ding, pp. 804–813, Univ. of Miss., University, Miss.
Anderson, M. (2003), Bioavailability, resuspension and control of sediment-borne nutrients in the Salton Sea, report, Colo. River Basin Reg. Water Quality Control Board, Dep. of Environ. Sci. Univ. of Calif., Riverside, Calif.
Arulanandan, K. (1975), Fundamental aspects of erosion of cohesive soils, *J. Hydraul. Div. Am. Soc. Civ. Eng.*, *101*, 635–639.
Blom, G., E. H. S. Vanduin, R. H. Aalderink, L. Lijklema, and C. Toet (1992), Modeling sediment transport in shallow lakes—Interactions between sediment transport and sediment composition, *Hydrobiologia*, *235–236*, 153–166, doi:10.1007/BF00026208.
Bombardelli, F. A., and M. H. García (2001), Three-dimensional hydrodynamic modeling of density currents in the Chicago River, Illinois, *Rep. 68*, Dep. of Civ. and Environ. Eng. Univ. of Ill. at Urbana-Champaign, Urbana, Ill.
Celik, I., and W. Rodi (1984), A deposition entrainment model for suspended sediment transport, *Rep. SFB 210/T/6*, Univ. Karlsruhe, Karlsruhe, Germany.
Coastal Engineering Research Center (CERC) (1984), Shore protection manual, U. S. Army Corps of Eng., Washington, D. C.
Chanson, H., M. Takeuchi, and M. Trevethan (2006), Using turbidity and acoustic backscatter intensity as surrogate measures of suspended sediment concentration. Application to a sub-tropical estuary (Eprapha Creek), report, Univ. of Queensland, Brisbane, Queensland, Australia.
Chow-Fraser, P. (1999), Seasonal, interannual, and spatial variability in the concentrations of total suspended solids in a degraded coastal wetland of Lake Ontario, *J. Great Lakes Res.*, *25*, 799–813.
Cook, C. B. (2000), Internal dynamics of a terminal basin lake: A numerical model for management of the Salton Sea, Ph.D. dissertation, Univ. of Calif., Davis.
Cook, C. B., G. T. Orlob, and D. W. Huston (2002), Simulation of wind-driven circulation in the Salton Sea: Implications for indigenous ecosystems, *Hydrobiologia*, *473*, 59–75, doi:10.1023/A:1016517331869.
Cozar, A., J. A. Galvez, V. Hull, C. M. Garcia, and S. A. Loiselle (2005), Sediment resuspension by wind in a shallow lake of Esteros del Ibera (Argentina): A model based on turbidimetry, *Ecol. Modell.*, *186*, 63–76, doi:10.1016/j.ecolmodel.2005.01.020.

Evans, R. D. (1994), Empirical evidence of the importance of sediment resuspension in lakes, *Hydrobiologia*, *284*, 5–12, doi:10.1007/BF00005727.

Freire, P., and C. Andrade (1999), Wind-induced sand transport in Tagus estuarine beaches—First results, *Aquat. Ecol.*, *33*, 225–233, doi:10.1023/A:1009911012260.

García, M. H. (1999), Sedimentation and erosion hydraulics, in *Hydraulic Design Handbook*, edited by L. W. Mays, pp. 6.1–6.113, McGraw-Hill, New York.

García, M. H., and G. Parker (1991), Entrainment of bed sediment into suspension, *J. Hydraul. Eng.*, *117*, 414–435, doi:10.1061/(ASCE)0733-9429(1991)117:4(414).

García, M. H., and G. Parker (1993), Experiments on the entrainment of sediment into suspension by a dense bottom current, *J. Geophys. Res.*, *98*, 4793–4807, doi:10.1029/92JC02404.

Gartner, J. W. (2004), Estimating suspended solids concentrations from backscatter intensity measured by acoustic Doppler current profiler in San Francisco Bay, California, *Mar. Geol.*, *211*, 169–187, doi:10.1016/j.margeo.2004.07.001.

Gill, A. E. (1982), *Atmosphere-Ocean Dynamics*, Academic, San Diego, Calif.

Gippel, C. J. (1989), The use of turbidimeters in suspended sediment research, *Hydrobiologia*, *176–177*, 465–480, doi:10.1007/BF00026582.

Gippel, C. J. (1995), Potential of turbidity monitoring for measuring the transport of suspended-solids in streams, *Hydrol. Processes*, *9*, 83–97, doi:10.1002/hyp.3360090108.

Gloor, M., A. Wuest, and M. Munnich (1994), Benthic boundary mixing and resuspension induced by internal seiches, *Hydrobiologia*, *284*, 59–68, doi:10.1007/BF00005731.

Hamilton, D. P., and S. F. Mitchell (1996), An empirical model for sediment resuspension in shallow lakes, *Hydrobiologia*, *317*, 209–220, doi:10.1007/BF00036471.

Hawley, N. (2004), A comparison of suspended sediment concentrations measured by acoustic and optical sensors, *J. Great Lakes Res.*, *30*, 301–309.

Hawley, N., B. M. Lesht, and D. J. Schwab (2004), A comparison of observed and modeled surface waves in southern Lake Michigan and the implications for models of sediment resuspension, *J. Geophys. Res.*, *109*, C10S03, doi:10.1029/2002JC001592.

Holdren, G. C., and A. Montaño (2002), Chemical and physical limnology of the Salton Sea—1999, report, Bur. of Reclam, U. S. Dep. of the Inter., Denver, Colo.

Horikawa, K. (1978), *Coastal Engineering: An Introduction to Ocean Engineering*, Univ. of Tokyo Press, Tokyo.

Hsu, T. W., H. K. Chang, and C. M. Hsieh (2003), A two-phase flow model of wave-induced sheet flow, *J. Hydraul. Res.*, *41*, 299–310.

James, R. T., J. Martin, T. Wool, and P. F. Wang (1997), A sediment resuspension and water quality model of Lake Okeechobee, *J. Am. Water Resour. Assoc.*, *33*, 661–680, doi:10.1111/j.1752-1688.1997.tb03540.x.

Jin, K. R., and K. H. Wang (1998), Wind generated waves in Lake Okeechobee, *J. Am. Water Resour. Assoc.*, *34*, 1099–1108, doi:10.1111/j.1752-1688.1998.tb04157.x.

Julien, P. Y. (1998), *Erosion and Sedimentation*, Cambridge Univ. Press, New York.

Jurg, B. (1996), Towards a new generation of sediment traps and a better measurement/understanding of settling particle flux in lakes and oceans: A hydrodynamical protocol, *Aquat. Sci.*, *58*, 283–296, doi:10.1007/BF00877472.

Kamphuis, J. W. (1975), Friction factor under oscillatory waves, *J. Waterw. Harbors Coastal Eng. Div.*, *101*, 135–144.

Keen, T. R., and Y. Furukawa (2007), A modular entrainment model for cohesive sediment, in *Estuarine and Coastal Fine Sediments Dynamics*, *Proc. Mar. Sci.*, vol. 8, edited by J. P.-Y. Maa, L. P. Sanford, and D. H. Schoellhamer, pp. 189–207, Elsevier, Amsterdam.

Knowlton, M. F., and J. R. Jones (1995), Temporal and spatial dynamics of suspended sediment, nutrients, and algal biomass in Mark Twain Lake, Missouri, *Arch. Hydrobiol.*, *135*, 145–178.

Kozerski, H. P. (1994), Possibilities and limitations of sediment traps to measure sedimentation and resuspension, *Hydrobiologia*, *284*, 93–100, doi:10.1007/BF00005734.

Kundu, P. K., and I. M. Cohen (2004), *Fluid Mechanics*, Academic, San Diego.

Lick, W., J. Lick, L. Jin, and J. Gailani (2007), Approximate equations for sediment erosion rates, in *Estuarine and Coastal Fine Sediments Dynamics*, edited by J. P.-Y. Maa, L. P. Sanford, and D. H. Schoellhamer, pp. 109–127, Elsevier, Amsterdam.

Lindstrom, M., L. Hakanson, O. Abrahamsson, and H. Johansson (1999), An empirical model for prediction of lake water suspended particulate matter, *Ecol. Modell.*, *121*, 185–198, doi:10.1016/S0304-3800(99)00081-2.

Linge, K. L., and C. E. Oldham (2002), Arsenic remobilization in a shallow lake: The role of sediment resuspension, *J. Environ. Qual.*, *31*, 822–828.

Lohrmann, A. (2001), Monitoring sediment concentration with acoustic backscattering instruments, report, Nortek, Annapolis, Md.

Luettich, R. A., D. R. F. Harleman, and L. Somlyody (1990), Dynamic behavior of suspended sediment concentrations in a shallow lake perturbed by episodic wind events, *Limnol. Oceanogr.*, *35*, 1050–1067.

Maa, J. P. Y., L. Sanford, and J. P. Halka (1998), Sediment resuspension characteristics in Baltimore harbor, Maryland, *Mar. Geol.*, *146*, 137–145, doi:10.1016/S0025-3227(97)00120-5.

Madsen, O. S., and W. D. Grant (1975), The threshold of sediment movement under oscillatory water waves: A discussion, *J. Sediment. Petrol.*, *45*, 360–361.

Mehta, A. J., T. M. Parchure, J. G. Dixit, and R. Ariathurai (1982), Resuspension Potential of Deposited Cohesive Sediment Beds, Academic, San Diego, Calif.

Mian, M. H., and E. K. Yanful (2003), Tailings erosion and resuspension in two mine tailings ponds due to wind waves, *Adv. Environ. Res.*, *7*, 745–765, doi:10.1016/S1093-0191(02)00027-8.

Mian, M. H., and E. K. Yanful (2004), Analysis of wind-driven resuspension of metal mine sludge in a tailings pond, *J. Environ. Eng. Sci.*, *3*, 119–135, doi:10.1139/s03-076.

Nielsen, P. (1992), *Coastal Bottom Boundary Layers and Sediment Transport*, World Sci, Singapore.

Nikora, V. I., and D. G. Goring (2002), Fluctuations of suspended sediment concentration and turbulent sediment fluxes in an open-channel flow, *J. Hydraul. Eng.*, *128*, 214–224, doi:10.1061/(ASCE)0733-9429(2002)128:2 (214).

Nortek (2004), AWAC user guide, Annapolis, Md.

Osborne, P. D., and B. Greenwood (1993), Sediment suspension under waves and currents—Time scales and vertical structure, *Sedimentology*, *40*, 599–622, doi:10.1111/j.1365-3091.1993.tb01352.x.

Parker, G. (2004), 1D sediment transport morphodynamics with applications to rivers and turbidity currents, e-book, Natl. Cent. for Earth Surf. Dyn., Minneapolis, Minn. (Available at http://cee.uiuc.edu/people/parkerg/)

Parker, G., C. M. Toro-Escobar, M. A. Ramey, and S. Beck (2003), The effect of floodwater extraction on the morphology of mountain streams, *J. Hydraul. Eng.*, *129*, 885–895, doi:10.1061/(ASCE)0733-9429(2003)129:11(885).

Raudkivi, A. J. (1998), *Loose Boundary Hydraulics*, 3rd ed., Pergamon Press, Oxford, U. K.

Reid, R. O. (1957), Modification of the quadratic bottom-stress law for turbulent channel flow in the presence of surface wind stress, *Tech. Memo. 93*, Beach Erosion Board, U.S. Army Corps of Eng., Washington, D. C.

Romero, J. R., et al. (2002), Seasonal water quality of shallow and eutrophic Lake Pamvotis, Greece: Implications for restoration, *Hydrobiologia*, *474*, 91–105, doi:10.1023/A:1016569124312.

Rosa, F., J. O. Nriagu, H. K. Wong, and N. M. Burns (1983), Particulate flux at the bottom of Lake Ontario, *Chemosphere*, *12*, 1345–1354, doi:10.1016/0045-6535(83)90139-X.

Sanford, L. P. (1992), New sedimentation, resuspension, and burial, *Limnol. Oceanogr.*, *37*, 1164–1178.

Sanford, L. P., and J. P. Y. Maa (2001), A unified erosion formulation for fine sediments, *Mar. Geol.*, *179*, 9–23, doi:10.1016/S0025-3227(01)00201-8.

Sheng, Y. P., and W. Lick (1979), Transport and resuspension of sediments in a shallow lake, *J. Geophys. Res.*, *84*, 1809–1826, doi:10.1029/JC084iC04p01809.

Shields, A. F. (1936), Anwendung der Aehnlichkeitsmechanik und der Turbulenzforschung auf die Geschiebebewegung, Ph.D. dissertation, Mitt. Preuss Ver. Anst., Berlin, (Application of similarity principles and turbulence research to bed-load movement, translation by W.P. Ott and J.C. van Uchelen, *Publ. 167*, Hydrodyn. Lab., Calif. Inst. of Technol., Pasadena, Calif., 1939.)

Smyth, C., and A. E. Hay (2002), Wave friction factors in nearshore sands, *J. Phys. Oceanogr.*, *32*, 3490–3498, doi:10.1175/1520-0485(2002)032<3490:WFFINS>2.0.CO;2.

Suk, N. S., Q. Guo, and N. P. Psuty (1998), Feasibility of using a turbidimeter to quantify suspended solids concentration in a tidal saltmarsh creek, *Estuarine Coastal Shelf Sci.*, *46*, 383–391, doi:10.1006/ecss.1997.0284.

Tostrud, M. B. (1997), The Salton Sea 1906–1996 computed and measured salinities and water level, report, Color. River Board of Calif, Glendale, Calif.

Van Rijn, L. C. (1984), Sediment transport: 2. Suspended-load transport, *J. Hydraul. Eng.*, *110*, 1613–1641, doi:10.1061/ (ASCE)0733-9429(1984)110:11 (1613).

Vogl, R. A., and R. N. Henry (2002), Characteristics and contaminants of the Salton Sea sediments, *Hydrobiologia*, *473*, 47–54, doi:10.1023/A:1016509113214.

Wang, K. H., K. R. Jin, and M. Tehrani (2003), Field measurement of flow velocities, suspended solids concentrations, and temperatures in Lake Okeechobee, *J. Am. Water Resour. Assoc.*, *39*, 441–456, doi:10.1111/j.1752-1688.2003.tb04397.x.

Weyhenmeyer, G. A., M. Meili, and D. C. Pierson (1995), Simple method to quantify sources of settling particles in lakes—Resuspension versus new sedimentation of material from planktonic production, *Mar. Freshwater Res.*, *46*, 223–231.

Wüest, A., N. H. Brooks, and D. M. Imboden (1992), Bubble plume modeling for lake restoration, *Water Resour. Res.*, *28*, 3235–3250, doi:10.1029/92WR01681.

Zyserman, J. A., and J. Fredsoe (1994), Data-analysis of bed concentration of suspended sediment, *J. Hydraul. Eng.*, *120*, 1021–1042, doi:10.1061/(ASCE)0733-9429(1994)120:9 (1021).

F. A. Bombardelli, E. G. Chung, and S. G. Schladow, Department of Civil and Environmental Engineering, University of California, 2001 Engineering III, One Shields Avenue, Davis, CA 95616, USA. (gschladow@ucdavis.edu)